Article

Bioactive Coating on Titanium Dental Implants for Improved Anticorrosion Protection: A Combined Experimental and Theoretical Study

Jozefina Katić [1], Ankica Šarić [2,*], Ines Despotović [3], Nives Matijaković [4], Marin Petković [5], and Željka Petrović [4,*]

[1] Department of Electrochemistry, Faculty of Chemical Engineering and Technology, University of Zagreb, Marulićev trg 19, 10000 Zagreb, Croatia; jkatic@fkit.hr (J.K.)

[2] Division of Materials Physics, Centre of Excellence for Advanced Materials and Sensing Device, Ruđer Bošković Institute, Bijenička cesta 54, 10002 Zagreb, Croatia; Ankica.Saric@irb.hr (A.Š.)

[3] Division of Physical Chemistry, Ruđer Bošković Institute, Bijenička cesta 54, 10002 Zagreb, Croatia; Ines.Despotovic@irb.hr (I.D.)

[4] Division of Materials Chemistry, Ruđer Bošković Institute, Bijenička cesta 54, 10002 Zagreb, Croatia; Nives.Matijakovic@irb.hr (N.M.); Zeljka.Petrovic@irb.hr (Ž.P.)

[5] Adentro dental studio, Petrova ul. 67, 10000 Zagreb, Croatia; info@adentro.hr (M.P.)

* Correspondence: Ankica.Saric@irb.hr (A.Š.); Zeljka.Petrovic@irb.hr (Ž.P.)

Abstract: In recent years extensive studies have been continuously undertaken on the design of bioactive and biomimetic dental implant surfaces due to the need for improvement of the implant-bone interface properties. In this paper, the titanium dental implant surface was modified by bioactive vitamin D3 molecules by self-assembly process in order to form an improved anticorrosion coating. Surface characterization of the modified implant was performed by field emission scanning electron microscopy (FE-SEM), attenuated total reflection-Fourier transform infrared spectroscopy (ATR-FTIR), and contact angle measurements (CA). Implant's electrochemical stability during exposure to an artificial saliva solution was monitored *in situ* by electrochemical impedance spectroscopy (EIS). Experimental results obtained were corroborated by means of quantum chemical calculations at the density functional theory level (DFT). The formation mechanism of the coating onto the titanium implant surface was proposed. During a prolonged immersion period, the bioactive coating effectively prevented the underlying titanium from corrosive attack (polarization resistance in order of $10^7 \ \Omega \ cm^2$) with ~95% protection effectiveness.

Keywords: titanium dental implant; vitamin D3; bioactive coating; anticorrosion protection; EIS; DFT

1. Introduction

Titanium and its alloys are the most commonly used implant materials and represent gold standards for dental implant fabrication due to their exceptional combination of high corrosion resistivity, favourable mechanical properties and biocompatibility [1-3]. Although the implantation success of titanium dental implants is high, complications still occur. There is increasing number of papers regarding titanium hypersensitivity, skin allergies like contact dermatitis, eczema, and immune reactions appearing after implant fixation [4-7]. It is also known that osseointegration problems in patients suffering from osteoporosis or other bone-related problems are one of reasons for unsuccessful implantation of dental implants [8]. Therefore, there is a need for continuous

45 improvement of dental implant material characteristics as well as their design to ensure long-term
46 integration of implants into the jaw.
47 Surface modification, which is in recent years in the focus of extensive research, is one of
48 strategies for improving corrosion resistivity, biocompatibility and bioactivity of dental implants
49 [3,8-10]. It was reported that the presence of inorganic coatings such as calcium phosphates [11] or
50 hydroxyapatite [12,13] promotes and accelerates bone formation in implant surroundings.
51 Nano-hydroxyapatite is used as a single coating or in a combination with collagen, bio glass or
52 titanium dioxide in a composite coating to imitate bio-environment of native bones [14].
53 Functionalization of the implant surfaces with organic or bioactive molecules will promote adhesion
54 of various cells [3]. Coatings based on bisphoshonates, drugs for bone disease treatments, act
55 osseoinductively and improve bone-implant connections [8,15,16].
56 According to currently available data, there is a great interest among dental surgeons and
57 implantologists for analyzing relationships between vitamin D3 and osseointegration process
58 [17,18]. Besides a known role of the vitamin D3 in bone metabolism, D3 is also very relevant for
59 normal functioning of the immune system what is of particular importance for a successful
60 integration of dental implant in surrounding bone tissue [17]. Therefore, in this study the titanium
61 dental implant surface was modified by bioactive vitamin D3 coating prepared by self-assembly
62 process. The main goal was (i) to make the dental implant surface more osseoinductive and
63 simultaneously (ii) more corrosion resistant during exposure to aggressive media (oral cavity fluids).
64 Based on the results of a combined electrochemical-theoretical study, bioactive coating formation
65 mechanism is clarified as well as coating influence on electrochemical behaviour of the titanium
66 implant during immersion in an artificial saliva solution. To the best of our knowledge, the present
67 study shows for the first time results of the integrated theoretical-experimental approach, which
68 contribute to a fundamental understanding of bioactive and protective coating formation and
69 predict overall electrochemical stability of modified dental implants in oral cavity fluids.
70

71 **2. Materials and Methods**

72 *2.1 Material and chemicals*

73 The Ankylos® C/X training implant A11 (length: 11 mm, diameter: 3.5 mm, Dentsply Friadent
74 GmbH, Germany), denoted as Ti-implant, was the object of the study and it was used as-received.
75 According to manufacturer's data, the implant is made of pure titanium grade 2, ISO 5832-2:2018 [19]
76 and its chemical composition is presented in Table 1 [20].
77 Vitamin D3 drops (ChildLife®, USA) was used as received. 122 μmol dm^{-3} cholecalciferol
78 (vitamin D3) in aqueous glycerol solution was used for modification of the Ti-implant surface. The
79 chemical structure of the vitamin D3, $C_{27}H_{44}O$, is presented in Fig. 1.
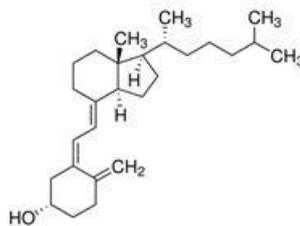
80
81 **Figure 1.** The chemical structure of the vitamin D3.

82 **Table 1**. Chemical composition (wt %) of titanium c.p. grade 2 [20].

Element	N	C	O	Fe	H	Ti	Other
%wt	0.03	0.10	0.25	0.30	0.0155	Balance	0.4

83 *2.2. Formation of bioactive coating*

84   Before modification, surface of as-received Ti-implant was ultrasonically cleaned with acetone
85   (p.a., Gram-Mol, Croatia) and redistilled water, degreased in absolute ethanol (p.a., Gram-Mol,
86   Croatia), and dried in a stream of nitrogen (99.999%, Messer, Germany). The D3 vitamin layer onto
87   the Ti-implant surface was prepared by self-assembly method. The Ti-implant was immersed in an
88   aqueous glycerol solution of vitamin D3 at 24 ± 2 °C during 24 hours. Afterwards, the coated
89   Ti-implant was dried in a regular air-convection oven (Instrumentaria, Croatia) at 70 °C for 5 hours.
90   That well-known procedure [21,22] enhanced the adhesion and stability of the coating due to the
91   conversion of the hydrogen-bonded intermediate into the stable coating with a chemical Ti-O bond
92   by an acid-base condensation mechanism. The formation mechanism as well as type of interactions
93   were accurately corroborated by DFT (section 3.3.). Finally,   the modified sample was rinsed with
94   absolute ethanol, redistilled water and dried in a stream of nitrogen. Thus prepared modified
95   sample, denoted in the text as the Ti-implant/bioactive coating, was used for further
96   characterization.

97   *2.3. Characterisation methods*

98   The morphology characteristics of unmodified and modified Ti-implant surfaces were
99   examined by a thermal field emission scanning electron microscope (model JSM-7000F, Jeol Ltd.,
100   Japan) at 15 kV.
101   The contact angles on investigated Ti-implant surfaces were measured with a drop of 1 μl
102   Milli-Q® water (Milli-Q® Direct 8 Water Purification System, Merck, Germany) at ambient
103   atmospheric conditions using a contact angle system OCA 20 (Dataphysics Instruments GmbH,
104   Germany). Values reported are the average of three measurements taken at smooth upper part of the
105   implant (without threads) after initial period of 10s-stabilization.
106   The ATR-FTIR measurements were performed by a Tensor II spectrometer (Bruker, USA) over
107   the range of 4000 – 340 cm^{-1} at 4 cm^{-1} scan step and total 16 scans per measurement.
108   Electrochemical characterization of unmodified and modified Ti-implant samples was assessed
109   by electrochemical impedance spectroscopy (EIS). A standard three-electrode cell (Corrosion Cell
110   6.1415.250, volume 50-150 mL, Metrohm, Autolab, USA) was utilized with the Ti-implant material
111   as a working electrode (an area of 0.98 cm^2 exposed to the electrolyte solution). Large-area Pt
112   electrode served as a counter electrode and   a reference electrode, to which all potentials in the
113   paper are referred, was an Ag|AgCl, 3.0 mol dm^{-3} KCl (E = 0.210 V vs. standard hydrogen electrode,
114   SHE). Barrier properties of unmodified and modified Ti-implants were evaluated in solution based
115   on the Fusayama artificial saliva (0.4 g dm^{-3} NaCl, 0.4 g dm^{-3} KCl, 0.6 g dm^{-3} $CaCl_2 \cdot 2H_2O$, 0.58 g dm^{-3}
116   $Na_2HPO_4 \cdot 2H_2O$, and 1 g dm^{-3} urea), pH 6.8 [23], prepared from p.a. grade chemicals and redistilled
117   water. Prior to   EIS measurements, the Ti-implant electrode was stabilized for 1 hour, 1 and 7 days
118   at the open circuit potential, E_{OC} in the electrolyte solution.
119   EIS measurements were performed subsequently in the frequency range from 10^5 to 10^{-3} Hz at
120   E_{OC} with an *ac* voltage amplitude of ±5 mV using Solartron 1287 potentiostat/galvanostat with
121   Solartron FRA 1260 (Solartron Analytical, UK) controlled by *ZPlot*® software (v. 3.5e, Southern Pines,
122   USA). The complex non-linear least squares (CNLS) fit analysis software [24] was employed to
123   model the experimental data obtained. The values of the elements of the proposed electric
124   equivalent circuit (EEC) were derived with χ^2 values less than 5×10^{-3} (errors in parameter values of
125   1–3%) using *ZView*® software (v. 3.5e, Southern Pines, USA).

126   *2.4. Computational details*

127   All calculations were performed by means of quantum chemical calculations at the density
128   functional theory (DFT) level using the Gaussian 09 program (revision D1) [25]. The small $(TiO_2)_{10}$
129   nanocluster served as a credible model for all possible molecular surface/bioactive molecule
130   interaction predictions [26,27]. The M06 functional designed by the Truhlar's group has been
131   selected [28-30]. For the geometry optimization the 6-31+G(d,p) + LANL2DZ basis set was utilized,
132   which means that the Pople's 6-31+G(d,p) double-ξ basis set was chosen for O, H, C atoms and the
133   LANL2DZ basis for the transition-metal (Ti) atoms [31]. Frequency calculations were done under

134   the harmonic approximation on all the optimized structures at the same level of theory with no
135   scaling in order to confirm the true minima of the structures. The final single point energies were
136   obtained using a highly flexible 6-311++G(2df,2pd) basis set for the O, H, C atoms, while the same
137   LANL2DZ ECP type basis set for titanium atoms was employed. To evaluate the bulk solvent
138   effects (1,2-ethandiol as a glycerol approximation, ε = 40.245), the implicit SMD polarizable
139   continuum solvation model [32] has been employed.
140   The Gibbs free energy interactions, ΔG^*_{INT} were computed as the difference between the total
141   free energy (G^*_{AB}) of the resulting (AB) structure and the sum of the total free energies ($G^*_A + G^*_B$) of
142   the associating units A and B.
143   The topological analysis of the charge density distribution was performed by employing
144   AIMALL software package [33] using the Bader's quantum theory of atoms in molecules (QTAIM)
145   [34] with SMD/M06/6-31+G(d,p) + LANL2DZ wave function derived from the optimization. Detail
146   description of the computational modelling is given in Supplementary Material.

3. Results and Discussion

148   *3.1. Surface characterization of the unmodified and modified Ti-implant samples*

149   A surface morphology of both unmodified (as-received Ti-implant) and modified
150   (Ti-implant/bioactive coating) samples was investigated by using FE-SEM and is presented in Fig. 2.
151   SEM images of the Ti-implant surface present inhomogeneous microstructured surface layer
152   exhibiting different size cavities and defects and is characterized by overall microroughness (Figs.
153   2ab). According to the manufacturer's data, the implant surface was grit-blasted and
154   high-temperature etched and this microstructure is commercially known as Friadent® plus
155   microstructure. The resulting surface favors the highly rapid apposition of bone-inducing cells on
156   the implant [19]. Observed morphology is in accordance with SEM results reported by R. Smeets at
157   al. [8], F. Rupp et al. [35], and T.J. Webster et al. [36]. The surface morphology did not change
158   significantly upon the bioactive coating on the Ti-implant surface preparation. Since the D3 layer
159   thickness is about 0.6 nm, according to the DFT results, the level of possible morphology
160   differentiation by SEM is very low.

161
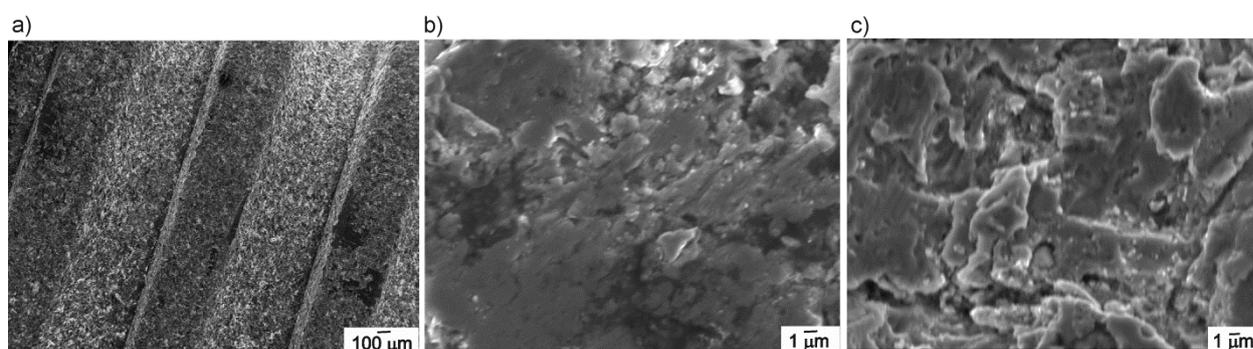
Figure 2. SEM images of the unmodified Ti-implant surface at: (a) 50x; (b) 3000x, and (c) of the
Ti-implant/bioactive coating surface at 3000x magnification.

165   A surface chemistry of the unmodified (Ti-implant) and modified (Ti-implant/bioactive
166   coating) samples was examined by ATR-FTIR and recorded spectra are presented in Fig. 3a. The
167   spectrum of the Ti-implant/bioactive coating sample was recorded immediately after the final step of
168   the coating formation (see section 2.2). A confirmation of a successful formation of the bioactive
169   coating on the Ti-implant surface was deduced based on the presence of vitamin D3 functional
170   group bands in investigated samples spectra, which indicates chemisorption on the Ti-implant
171   surface, as will be given below.
172   In the Ti-implant sample ATR-FTIR spectrum, a broad band observed at 3305 cm^{-1} is
173   characteristic to the stretching vibration of adsorbed water on the Ti-implant surface. A vibration

174 band characteristic for the Ti-OH appeared at 1029 cm^{-1}. Band at 1421 cm^{-1} was arisen from TiO$_2$
175 lattice vibration and bands locating in the range from 350 – 1000 cm^{-1} are related to the Ti-O
176 stretching vibrations [37,38]. According to described bands, the Ti-implant surface is covered by a
177 TiO$_2$ layer.
178   In Fig. 3a a spectrum of the Ti-implant/bioactive coating sample is presented. ATR-FTIR spectra
179 of vitamin D3 and glycerol were also recorded since vitamin D3 drops used for the bioactive coating
180 formation contain glycerol as a solvent, Fig. 3b. As can be seen, spectra of both compounds are very
181 similar and are in accordance with the literature data [39]. A clear difference is a peak at 1643 cm^{-1}
182 that is assigned to the H-C=CH stretching vibrations characteristic to the vitamin D3.
183   A spectrum of the Ti-implant/bioactive coating (Fig. 3a)   contains observed distinctive bands
184 for vitamin D3 and glycerol. A presence of broader band at 1627 cm^{-1}, characteristic for vitamin D3
185 molecule, confirms a successful formation of the vitamin D3 layer on the Ti-implant surface. Shifts of
186 all bands to lower wavenumbers also indicate an attachment (chemisorption) of vitamin D3
187 molecules to the Ti-implant surface.. A peak at 351 cm^{-1} of TiO$_2$ is visible due to relatively low D3
188 layer thickness according to the DFT results.
189   Since the ATR-FTIR spectra of D3 and glycerol molecules exhibited high degree of resemblance
190 and intermolecular interactions exist between both molecules (DFT results, section 3.3.), there is a
191 possibility that both compounds are simultaneously bonded to the implant surface as a two
192 layer-structured coating, as will be discussed later (section 3.3.). Therefore, it is impossible to
193 accurately determine interaction type and nature between vitamin D3 molecule and Ti-implant
194 substrate only from the observed band shifts. Further experimental characterization as well as
195 theoretical by means DFT calculations were carried out to accurately determine the structure of the
196 bioactive coating formed onto the Ti-implant surface.
197

198
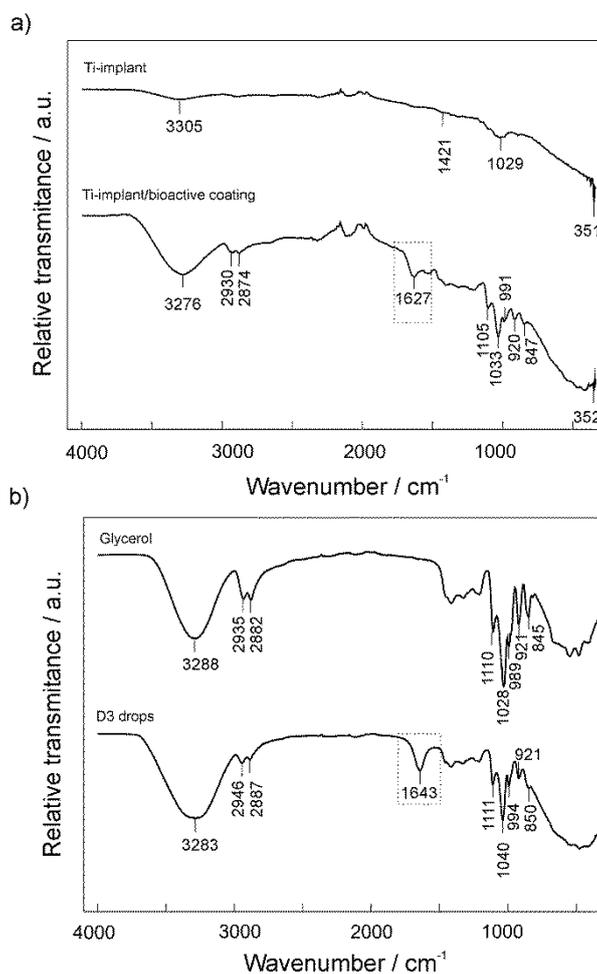
199 **Figure 3.** ATR-FTIR spectra of (a) the unmodified and modified Ti-implant surfaces and (b) D3 drops
200 and glycerol.

201 A study of wetting properties of implant surfaces is very important for understanding of a
202 complex reaction series occurring during the initial contact between implant and body fluids [8,35].
203 In this study wettability measurements were conducted in order to evaluate level of a bioactive
204 coating formation success. A static contact angle of water, θ was measured on the unmodified
205 (Ti-implant) and modified Ti-implant (Ti-implant/bioactive coating) surfaces. Measurements were
206 carried out at upper smooth part of the implant body and corresponding micrographs are presented
207 in Fig. 4.
208 The higher value of contact angle, $\theta = 87.5 \pm 2.2°$ was obtained on the Ti-implant surface in
209 comparison to the value obtained on the Ti-implant/bioactive coating surface, $\theta = 60.4 \pm 1.5$. Wetting
210 properties of the Ti-implant surface were changed by a presence of a coating and these results were
211 confirmation of a successful formation of the bioactive coating on the implant surface. The surface
212 modification induced a change from hydrophobic (Ti-implant) to hydrophilic surface character
213 (Ti-implant/bioactive coating). Therefore, wetting properties of the modified Ti-implant surface are
214 predominantly affected by the hydrophilic –OH functional groups oriented in the upper part of the
215 coating, possibly originating from glycerol molecules, as will be discussed on the basis of DFT
216 results (see section 3.3.).

217
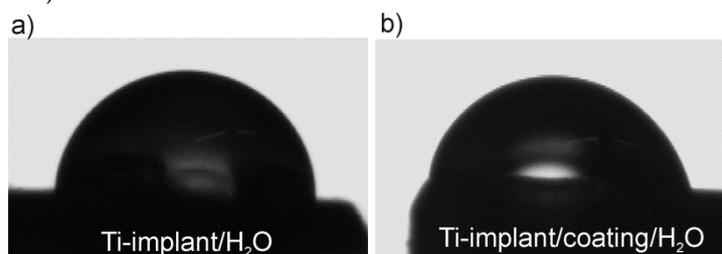
218 **Figure 4.** Optical micrographs of a water drop on (a) the Ti-implant surface and (b) the
219 Ti-implant/bioactive coating surface.

220

221 *3.2. Electrochemical characterization of the unmodified and modified Ti-implant samples*

222 The electrochemical behaviour of the unmodified and D3 vitamin modified Ti-implant surfaces,
223 as one of prerequisite factors for dental implant biocompatibility in contact with aggressive oral
224 cavity fluids and hence successful implantation process, was studied under *in vitro* conditions of real
225 dental implant application. Employing non-destructive method of electrochemical impedance
226 spectroscopy (EIS), electrochemical stability of investigated samples during different immersion
227 times (shown in Fig. 5) was monitored *in situ* in artificial saliva electrolyte solution at E_{OC} over the
228 wide frequency range and obtained impedance spectra are given in the form of Bode magnitude and
229 phase angle plots in Figs. 5ab. The impedance data were analyzed in terms of the electric equivalent
230 circuits, EECs presented in Figs. 5cd and the impedance parameter values are provided in Tables 2
231 and 3.
232 In the EECs employed, the constant-phase element, CPE was used to describe a non-ideal
233 capacitance behavior in order to compensate non-homogeneity in the system (inhomogeneous
234 current flow, capacitance dispersion, etc.) [40-42]. The impedance of CPE can be expressed as
235 $Z_{CPE}=[Q(j\omega)^n]^{-1}$ where Q and n are parameters associated with CPE. For CPE exponent $n=1$, the
236 frequency–independent CPE parameter Q represents the capacity of the interface. For $n \neq 1$, the
237 system shows behaviour that has been attributed to surface heterogeneity, presence of surface films,
238 or to continuously distributed time constants for charge-transfer reactions [40]. The corresponding
239 interface capacitance values were calculated according to the Brug's relation [41]:

$$Q = C^n(R_{\Omega}^{-1} + R^{-1})^{1-n}. \tag{1}$$

240 The EIS data of unmodified Ti-implant (Ti-implant/oxide film/artificial saliva interface) were
241 fitted to the EEC with two time constants (Fig. 5c) and parameter values are presented in Table 2.
242 The EEC used has been commonly used to analyze impedance results of Ti and Ti-alloys covered
243 with a bi-layer structure of the oxide film [22,43-48]. The high/middle frequency time constant
244 (R_1-CPE$_1$) describes the characteristics of the outer porous layer of the oxide film. R_1 represents the
245 resistance and CPE$_1$ the capacitance of the outer layer. The low frequency time constant (R_2-CPE$_2$)
246 is related to the inner barrier layer of the oxide film, predominately containing titanium(IV) oxide
247 [1,44,49]. R_2 represents the resistance and CPE$_2$ the capacitance of the barrier layer. R_Ω is the ohmic
248 (electrolyte) resistance. The polarization (corrosion) resistance, R_P is the sum of R_1 and R_2 resistance
249 contributions and determines overall corrosion resistance of the oxide-covered Ti-implant [50].
250
251

252
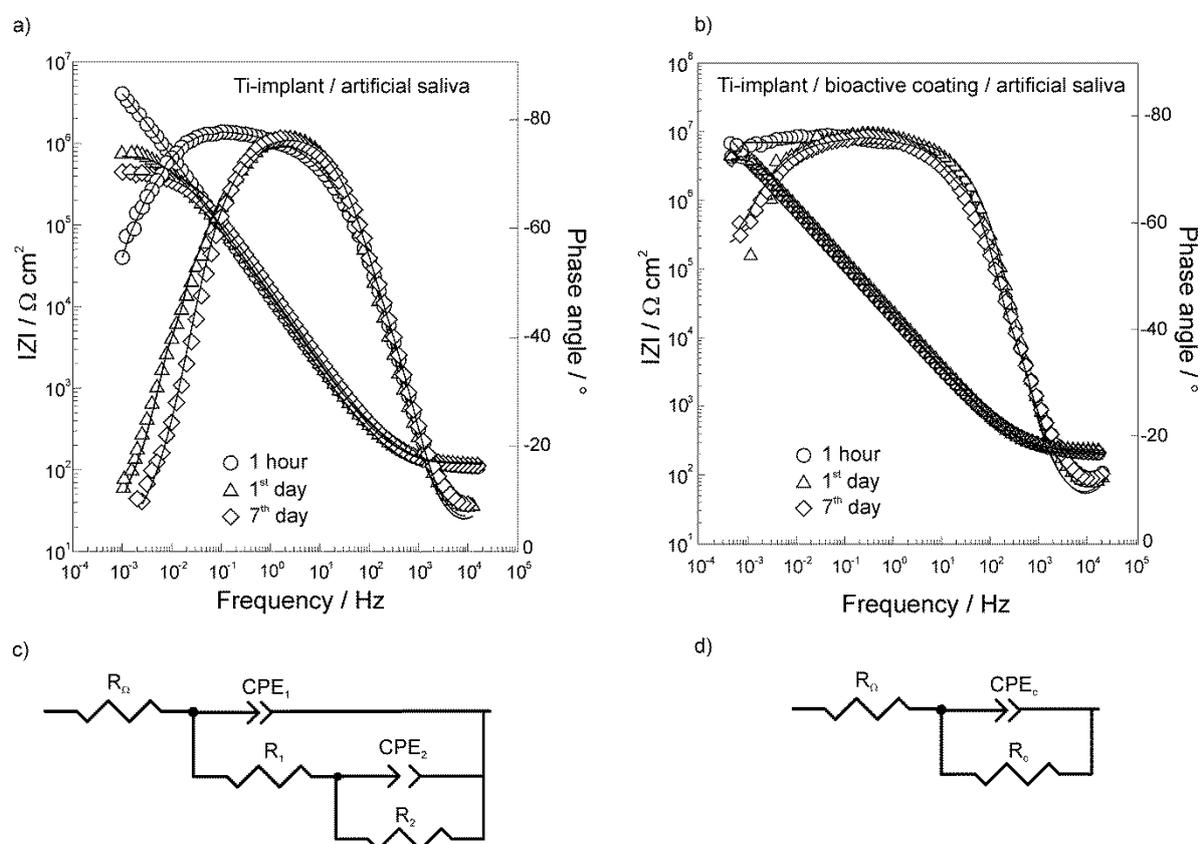
253

254 **Figure 5.** The Bode plots of (a) the unmodified Ti-implant and (b) the modified Ti-implant recorded
255 at E_{OC} in the artificial saliva electrolyte solution, pH 6.8 after various immersion times denoted.
256 Symbols: the experimental data; solid lines: the modeled data. The schematic presentation of the
257 electric equivalent circuits (EECs) used to fit the spectra of (c) the unmodified Ti-implant and (d) the
258 modified Ti-implant.

259

260 **Table 2**. Impedance parameters calculated for EIS data of the Ti-implant/oxide film/artificial saliva
261 interface (Fig. 5a) recorded at E_{OC} after various exposure times denoted.

Exposure time	R_Ω / Ω cm²	$10^6 \times Q_1$ / Ω^{-1} cm⁻² s^n	n_1	C_1 / μF cm²	R_1 / Ω cm⁻²	$10^6 \times Q_2$ / Ω^{-1} cm⁻² s^n	n_2	C_2 / μF cm⁻²	R_2 / MΩ cm²
1h	111	9.98	0.853	3.02	760	5.16	0.850	1.38	9.90

1 day	123	2.88	0.997	2.88	174	12.1	0.788	2.10	0.79
7 days	123	3.26	0.978	2.71	307	9.21	0.810	1.88	0.44

262
263
264　　　As can be seen from Fig. 5a and Table 2, electrochemical stability of the Ti-implant sample was
265　significantly decreased during an exposure to artificial saliva solution what was particularly
266　reflected in R_1 and R_2 values. During the initial short immersion period, an oxide film on the
267　Ti-implant surface possessed high protective properties (high R_P value). Since the artificial saliva
268　solution represents an aggressive medium, high amount of chloride ions affects oxide film
269　properties and acceleratess the titanium corrosion (degradation) process during prolonged
270　immersion period [51]. Calculated parameters, especially R_1 values indicate that the contribution of
271　the outer layer of the oxide film to the electrochemical behaviour is rather imperceptible, and the
272　overall EIS response is dominated by the inner barrier layer of the oxide film what is in accordance
273　with previously reported results [43,44].
274
275　　　The Bode plots of the Ti-implant/bioactive coating sample measured after specified artificial
276　saliva exposure times are presented in Fig. 5b. Brief inspection of the spectra points to the different
277　impedance behavior of vitamin D3 modified Ti-implant surface in comparison to the unmodified
278　Ti-implant surface. Hence, EEC with only one time constant was employed to analyze the EIS data
279　(Fig. 5d), with R_c and C_c attributed to the resistance and capacitance of the bioactive coating formed.
280　The bioactive coating structure is very compact and well-ordered due to the presence of vitamin D3
281　layer over the oxide covered Ti-implant surface as confirmed by the DFT calculation results (section
282　3.3) and both of layers contribute to the overall corrosion resistance of the underlying Ti-implant.
283　The resistance R_c also represents the polarization resistance,, $R_P$of the investigated system.. The fitted
284　values are presented in Table 3.
285

286　　　**Table 3**. Impedance parameters calculated for EIS data of the Ti-implant/oxide film/D3
287　layer/artificial saliva interface (Fig. 5b) recorded at E_{OC} after various exposure times denoted together
288　with protection effectiveness values

Exposure time	R_Ω / Ω cm²	$10^6 \times Q_c$ / Ω^{-1} cm⁻² sⁿ	n	C_c / μF cm⁻²	R_c / MΩ cm²	η / %
1 h	157	7.97	0.851	2.52	51.7	80.9
1 day	157	6.95	0.862	2.54	17.4	95.5
7 days	157	8.14	0.846	2.47	17.6	97.5

289
290
291　　　As can be seen, the dependence of phase angle versus log f points to a capacitive behaviour of
292　the coated Ti-implant sample over the wider frequency range in comparison to the unmodified
293　Ti-implant sample. Besides, higher low frequency magnitude values that remain almost unchanged
294　during investigated period of 7 days indicate improved electrochemical stability and corrosion
295　protection of the Ti-implant upon bioactive coating formation.
296　　　However, deep insight into phase angle versus log f dependence, as structural sensitive
297　parameter, reflects possible structural changes inside the bioactive coating during first day of sample
298　immersion to the artificial saliva solution. This rearrangement/reorganization inside the bioactive
299　coating induced a slight deterioration of protective properties as can be seen from R_c values (Table
300　3). After prolonged immersion period (from 1st to 7th day), EIS responses did not change
301　significantly. Obviously, observed coating rearrangement/reorganization was induced by an initial

302 contact between modified Ti-implant surface and electrolyte solution. According to the literature,
303 structural reorganization that modulates electrical properties is known for self-assembled surface
304 layers and can be stimulated by potential or by polarity and wettability of terminal functional group
305 of the layer molecules [52,53]. On the basis of DFT calculations (section 3.3.), weak intermolecular
306 interactions between glycerol and D3 molecules are present and they result in orienting of glycerol
307 molecules in the outer part of the bioactive coating. Thus, glycerol –OH terminal functional groups
308 affect polarity and wettability of the coating formed on the Ti-implant surface what it was observed
309 in the contact angle value (Fig. 4). Probably, there is a possibility of stronger interactions between
310 glycerol –OH group and electrolyte components that caused a glycerol withdrawal from the
311 Ti-implant surface and simultaneous structural changes inside the bioactive coating as was
312 confirmed by DFT (section 3.3.). The coated Ti-implant surface was perturbed and small defects in
313 the coating structure probably occurred. Consequently, ions/water molecules could penetrate into
314 the coating hence causing a decrease in R_c value after 1 day-immersion. During this first day, the
315 coating structure again achieved the most stable conformation resulting in unchanged R_c values. It
316 should be stressed out, albeit the R_P value decrease was observed due to the structural organization
317 occurrence, the overall coating resistance (the sum of oxide film + D3 layer resistances), inversely
318 proportional to the corrosion rate, remained in order of 10^7 Ω cm^2 imparting a sufficient corrosion
319 protection to the underlying Ti-implant material.
320
321 The corrosion protection effectiveness, η of the bioactive coating formed on the Ti-implant
322 surface was calculated using the relation:

$$\eta = (R_{p(modified)} - R_{p(umodified)})/R_{p(modified)} \qquad (2)$$

323 where $R_{p,(unmodified)}$ and $R_{p,(modified)}$ are the polarization resistances of unmodified and modified
324 Ti-implant. The protection effectiveness values are presented in Table 3.
325 According to EIS results, protective properties of the unmodified, as-received Ti-implant
326 (Ti-implant/oxide film) were significantly deteriorated during its immersion into an artificial saliva
327 solution. On the other hand, the D3 layer, prepared by self-assembly process on the oxide-covered
328 Ti-implant surface (Ti-implant/bioactive coating), behaved as an excellent barrier to the transport of
329 corrosive ions/molecules from the bulk electrolyte to the Ti-implant surface during a prolonged
330 exposure. Additionally, vitamin D3 molecules are bioactive molecules that can promote and
331 accelerate an osseointegration process. Thus this bioactive, and at the same time, highly protective
332 coating can serve as a good candidate for biocompatible Ti dental implants enabling a pivotal role in
333 successful implantation process.

334

335 *3.3. Formation mechanism of bioactive implant coating*

336 Notwithstanding the part of the formation mechanism that has been discussed above
337 considering experimental results, more detail theoretical study of Ti-implant surface/bioactive
338 molecule interactions is still needed to fully clarify the coating formation mechanism. The
339 experimental findings were corroborated by means of DFT calculations based on effects of
340 cholecalciferol (D3 vitamin) as well as glycerol as its alcoholic solvent in pharmaceutical
341 composition of vitamin D3 solution. The small $(TiO_2)_{10}$ nanocluster served as a credible model for
342 all possible molecular Ti-implant surface/bioactive molecule interaction predictions [26,27]. There is
343 a possibility that the presence of other kinds of Ti-implant surface/molecule interactions (due to the
344 presence of glycerol solvent) except the $(TiO_2)_{10}$–cholecalciferol interaction could be responsible for
345 influencing the coating formation mechanism. Hence, the implant surface/bioactive molecule
346 interactions were investigated considering the results obtained from a computational study of
347 Gibbs free energies of $(TiO_2)_{10}$–cholecalciferol, $(TiO_2)_{10}$–cholecalciferol–glycerol, as well as
348 $(TiO_2)_{10}$–glycerol molecular interactions (ΔG^*_{INT}). One should mention that only the
349 thermodynamically most stable structures are discussed here.

350   Different binding interactions were established, involved in the processes of the
351 (TiO$_2$)$_{10}$—cholecalciferol interaction. The interactions, which involve Ti—O bonding and C—H···O
352 hydrogen bonding, are shown in Figure 6. When Ti—O and hydrogen bonds were formed, the free
353 energies of (TiO$_2$)$_{10}$—cholecalciferol molecular interactions were released (ΔG^{*}_{INT} = -6.64 kcal mol^{-1}).
354 The (TiO$_2$)$_{10}$—cholecalciferol interaction has been found to be a spontaneous exergonic process. The
355 formation of such completely enclosed structure of (TiO$_2$)$_{10}$—cholecalciferol, with high coverage
356 level of the (TiO$_2$)$_{10}$ surface, was likely a consequence of the synergistic effect of all the interactions
357 mentioned above. Namely, the most stable structure of (TiO$_2$)$_{10}$—cholecalciferol possesses Ti—O
358 bond ($d_{Ti—O}$= 2.252 Å, $E_{Ti—O}$= -14.68 kcal mol^{-1}) which is stabilized by eleven weaker C—H···O
359 hydrogen bonds ($E_{O···H}$ ranges from -0.61 kcal mol^{-1} to -2.99 kcal mol^{-1}; $d_{O···H}$ ranges from 3.295 Å to
360 2.358 Å). The Ti—O bond is attributed to an ionic (polar coordinate) type of interacting according to
361 $\Delta^2\rho\,(r_c)$> 0 and $H(r_c)$ > 0.
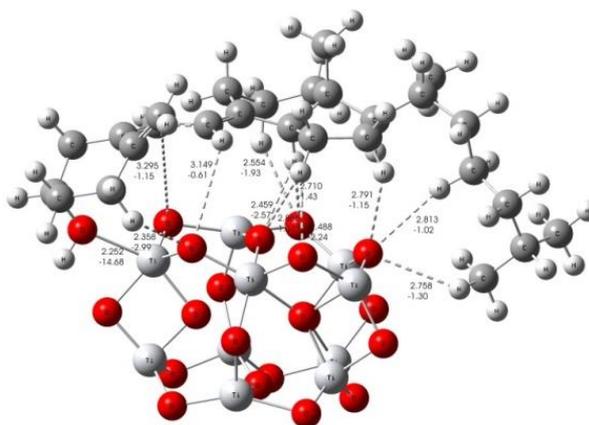
362

363   **Figure 6**. The most stable structure of the (TiO$_2$)$_{10}$—cholecalciferol (vitamin D3) predicted by DFT;
364   selected values of bond distances in Å and bond energies in kcal mol^{-1}.

365   The possible formation of the (TiO$_2$)$_{10}$—cholecalciferol—glycerol structure involved different
366 binding interactions in relation to the (TiO$_2$)$_{10}$—cholecalciferol formation mechanism. That difference
367 is probably a consequence of higher steric as well as energetic requirements needed for the
368 (TiO$_2$)$_{10}$—cholecalciferol—glycerol molecular interactions. These interactions require an additional
369 step of releasing a few C—H···O hydrogen bonds in stable (TiO$_2$)$_{10}$—cholecalciferol structure (Fig. 6)
370 due of the access of one or more glycerol molecules. Namely, when
371 (TiO$_2$)$_{10}$—cholecalciferol—glycerol was formed, the cholecalciferol could be attached to the (TiO$_2$)$_{10}$
372 cluster in different way related to (TiO$_2$)$_{10}$—cholecalciferol structure, as shown in Figs. 6 and 7. It is
373 important to note the large capacity of the cholecalciferol in (TiO$_2$)$_{10}$—cholecalciferol structure to
374 attract glycerol molecule due to stronger O—H···O hydrogen and weaker C—H···O hydrogen bonds
375 ($E_{O···H}$ ranges from -0.82 kcal mol^{-1} to -1.86 kcal mol^{-1}; $d_{O···H}$ ranges from 2.963 Å to 2.524 Å), as shown
376 in Fig. 7. However, the formation of the (TiO$_2$)$_{10}$-cholecalciferol-glycerol structure is slightly
377 endergonic process (ΔG^{*}_{INT} = 5.51 kcal mol^{-1}) indicating that it could act only as a "coating
378 intermediate", which is in a good agreement with FT-IR spectroscopy and contact angle
379 measurement results (Figs. 3 and 4). The most probably, as can be seen from the EIS response after 1
380 day-immersion of the modified Ti-implant (Fig. 5b), this "coating intermediate" was responsible for
381 temporal coating structural rearrangement that was reflected in the coating resistance value (R_c
382 value, Table 3).

383
384   **Figure 7**. The most stable structure of the $(TiO_2)_{10}$—cholecalciferol (vitamin D3)-glycerol, predicted
385   by DFT; selected values of bond distances in Å and bond energies in kcal mol^{-1}.

386   Based on experimental findings and DFT calculations, it seems that is not possible to predict
387   the mechanism responsible for bioactive coating formation in the presence of solvent molecules
388   solely based on the aspect of thermodynamic stability of the coating intermediate. For more
389   detailed/accurate coating formation mechanism, additional species present in the artificial saliva
390   solution (simulated oral cavity physiological solution) should be taken into consideration due to
391   their possible stronger coordination ability, which could replace weaker hydrogen bonds between
392   cholecalciferol and glycerol.
393
394   Taking into account the calculated energy values of common bonding (Ti—O) and eleven
395   weaker C—H···O hydrogen bonds, as well as ΔG^*_{INT}, it can be concluded that cholecalciferol (D3
396   vitamin) molecules bond to the oxide-covered Ti implant surface displaying high coverage level.
397   Consequently, the bioactive coating on the Ti dental implant surface is very stable and resistant to
398   the aggressive environment of artificial saliva according to the EIS findings. Because of well-known
399   bioactivity and in this study proofed protective effectiveness of D3 vitamin as a coating, a described
400   strategy can be applied for a design of real dental implants of improved biocompatibility and
401   osseointegrity.
402
403

404   **4. Conclusions**

405   In this study, the titanium dental implant was functionalized with bioactive molecules of
406   vitamin D3 (cholecalciferol) to make its surface more corrosion resistant to aggressive oral cavity
407   fluids and at the same time more attractive for bone cells adhesion. An integrated
408   experimental-theoretical approach for characterization of the Ti dental implant/bioactive coating
409   interface was applied.
410   ATR-FTIR spectroscopy and contact angle measurement results confirmed the presence of the
411   D3 layer onto the oxide covered Ti-implant surface.
412   Coating's formation mechanism was proposed considering the DFT calculation results. D3
413   molecules possess an affinity to the titanium surface covered by the TiO_2 layer and they are bonded
414   to the surface through a Ti—O bond ($E_{Ti—O}$= -14.68 kcal mol^{-1}), which is stabilized by eleven weaker
415   C—H···O hydrogen bonds ($E_{O···H}$ ranges from -0.61 kcal mol^{-1} to -2.99 kcal mol^{-1}). This type of
416   interactions resulted in a formation of the enclosed Ti-implant surface–vitamin D3 structure with
417   high surface coverage level.
418   The bioactive coating influence on protective properties of the Ti-implant was investigated *in*
419   *situ* by using EIS during different exposure times to an artificial saliva solution. The presence of the
420   D3 layer on the oxide covered Ti-implant surface significantly changed the structure of the

421 electrified Ti-implant surface/bioactive coating/artificial saliva interface compared to the Ti-implant
422 surface/oxide film/artificial saliva interface.
423   During a prolonged immersion period the stable bioactive coating effectively prevented the
424 Ti-implant surface from contacting aggressive ions in the artificial saliva solution. After 7
425 day-immersion period, the protection effectiveness amounted 97.5%.
426   Dental implant design that simultaneously stimulates an implant-bone connection creation
427 (osseointegration) and enables a good anticorrosion protection during an exposure to oral cavity
428 fluids is desirable from a real applicable point of view.
429

430 **Supplementary Materials:** The following are available online, Computational modelling, Table S1: Formation
431 of the most stable $(TiO_2)_{10}$−cholecalciferol[a], $(TiO_2)_{10}$−cholecalciferol−glycerol [b] and $(TiO_2)_{10}$−glycerol species[c].
432 Standard state (1M) free energies of interaction $\Delta_r G^*_{INT}$ computed by using the SMD solvation model at the
433 M06/6-311++G(2df,2pd) + LANL2DZ// M06/6-31+G(d,p) + LANL2DZ level of theory, Table S2: Bond lengths (*d*),
434 energies (*E*) and QTAIM properties of the selected bonds in the most stable $(TiO_2)_{10}$−cholecalciferol,
435 $(TiO_2)_{10}$−cholecalciferol−glycerol and $(TiO_2)_{10}$−glycerol structures, Table S3: Total electronic energy, E^{Tot}_{soln},
436 obtained at the SMD/M06/6-311++G(2df,2pd) + LANL2DZ//SMD/M06/6-31+G(d,p) + LANL2DZ level of theory,
437 thermal correction to the Gibbs free energy, $\Delta G^*_{VRT,soln}$, obtained at the SMD/M06/6-31+G(d,p) + LANL2DZ level
438 of theory, and total free energy, G^*_X, $(G^*_X = E^{Tot}_{soln} + \Delta G^*_{VRT,soln})$ in 1,2-ethandiol media of the investigated species
439 (all energies in hartree), Table S4: Optimized Cartesian coordinates of the calculated systems (given as XYZ
440 format).
441

454

455 **References**

456

457 1. Eliaz, N. Corrosion of Metallic Biomaterials: A Review. *Materials* **2019**, *12*, 2019, 12, 407-498.,
458   doi:10.3390/ma12030407.
459 2. Hansen, D.C. Metal Corrosion in the Human Body: The Ultimate Bio-Corrosion Scenario. *Electrochem. Soc.*
460   *Interface* **2008**, *17*, 31-35.
461 3. Gaviria, L,; Salcido, J.P.; Guda, T.; Ong, J.L. Current trends in dental implants. *J. Korean Assoc. Oral.*
462   *Maxillofac. Surg.* **2014**, *40*, 50-60., doi: 10.5125/jkaoms.2014.40.2.50.
463 4. Yan, H.; Afroz, S.; Dalanon, J.; Goto, N.; Hosoki, M. Metal allergy patient treated by titanium implant
464   denture: A case report with at least 4-year follow up. *Clinical Case Reports* **2018**, *6*, 1972-1977., doi:
465   10.1002/ccr3.1753.
466 5. Siddiqi, A.; Payne, A.G.T.; De Silva, R.K.; Duncan, W.J. Titanium allergy: could it affect dental implant
467   integration?. *Clin. Oral Impl. Res.* **2011**, *22*, 673–680., doi: 10.1111/j.1600-0501.2010.02081.x.
468 6. Syed, M.; Chopra, R.; Sachdev, V. Allergic Reactions to Dental Materials-A Systematic Review. *J. Clin.*
469   *Diagnostic Research* **2015**, *9*, ZE04-ZE09., doi: 10.7860/JCDR/2015/15640.6589.

470 7.   Sicilia, A.; Cuesta, S.; Coma, G.; Arregui, I.; Guisasola, C.; Ruiz, E.; Maestro, A. Titanium allergy in dental
471   implant patients: a clinical study on 1500 consecutive patients. *Clin. Oral Impl. Res.* **2008**, *19*, 823–835., doi:
472   10.1111/j.1600-0501.2008.01544.x.
473 8.   Smeets, R.; Stadlinger, B.; Schwarz, F.; Beck-Broichsitter, B.; Jung, O.; Precht, C.; Kloss, F.; Gröbe, A.;
474   Heiland, M.; Ebker, T. Impact of Dental Implant Surface Modifications on Osseointegration. *Bio. Med.*
475   *Research International* **2016**, *2*, 1-16., doi:10.1155/2016/6285620.
476 9.   Al Mugeiren, O.M.; Baseer, M.A. Dental implant Bioactive surface Modifiers: An Update. *J. Int. Soc. Prev.*
477   *Commmunity Dent.* **2019**, *9*, 1-4., doi: 10.4103/jispcd.JISPCD_303_18.
478 10. Tian, B.; Xie, D.B.; Wang, F.H. Corrosion behavior of TiN and TiN/Ti composite films on Ti6Al4V alloy in
479   Hanks solution. *J. Applied Electrochem.* **2009**, *39*, 447-453., doi: 10.1007/s10800-008-9696-4.
480 11. Yuan, H.; Yang, Z.; Li, Y.; Zhang, X.; De Bruijn, J.D.; De Groot, K. Osteoinduction by calcium phosphate
481   biomaterials. *J. Mater Sci. Mater. Med.* **1998**, *8*, 723-726., doi: 10.1023/A.1008950902.
482 12. Sousa, L.L.; Pereira Ricca, V.; Gouvêa Prado, D.; Chefer Apolinario, R.; de Oliveira Vercik, L.C.; da Silva
483   E.C.; Santos Fernandes, R.M.C.; Mariano, N.A. Titanium Coating with Hydroxyapatite and Chitosan
484   Doped with Silver Nitrate. *Mater. Res.* **2017**, *21*, 1-6., doi: 10.1590/1980-5373-MR-2017-0021.
485 13. Łukaszewska-Kuska, M.; Krawczyk, P.; Martyla, A.; Hędzelek, W.; Dorocka-Bobkowska, B.
486   Hydroxyapatite coating on titanium endosseous implants for improved osseointegration: Physical and
487   chemical considerations. *Advan. Clin. Exp. Med.* **2018**, *27*, 1055-1059., doi: 10.17219/acem/69084.
488 14. Choi, A.H.; Ben-Nissan, B.; Matinlinna, J.P.; Conway, R.C. Current perspectives: calcium phosphates
489   nanocoatings and nanocomposite coatings in dentistry. *J. Dent. Res.* **2013**, *92*, 853-859., doi:
490   10.1177/0022034513497754.
491 15. Rojo, L.; Gharibi, B.; McLister, R.; Meenan, B.J.; Deb, S. Self-assembled monolayers of alendronate on
492   Ti6Al4V alloy surfaces enhance osteogenesis in mesenchymal stem cells. *Nature Sci. Reports* **2016**, *6*,
493   30548-30557., doi: 10.1038/srep30548.
494 16. Hu, X.; Neoh, K.G.; Shi, Z.; Kang, E.T.; Wang, W. An In vitro Assessment of fibroblast and Osteoblast
495   Response to Alendronate-Modified titanium and the Potential for Decreasing Fibrous Encapsulation.
496   *Tissue Engineering A* **2013**, *19*, 1919-1928., doi: 10.1089/ten.tea.2012.0218.
497 17. Trybek, G.; Aniko-Wlodarczyk, M.; Kwiatek, J.; Preuss, O.; Brodkiewicz, A.; Sinicyn, A.; Grzywacz, A. The
498   effect of vitamin D3 on the osteointegration of dental implants. *Balt. J. Health Phys. Activity* **2018**, *10*, 25-33.,
499   doi: 10.29359/BJHPA.10.4.02.
500 18. Satue, M.; Monjo, M.; Ronold, H.J.; Lyngstadaas, S.P.; Ramis, J.M. Titanium implants coated with
501   UV-irradiated vitamin D precursor and vitamin E: in vivo performance and coating stability. *Clin. Oral*
502   *Impl. Res.* **2016**, *28*, 1-8., doi: 10.1111/clr.12815.
503 19. Ankylos® Bibliography No 6-252047/007, Implanting Brilliancy, Friadent GmbH, Mannheim, Germany;
504   https://www.iso.org/standard/69907.html (accessed on 1st July 2019).
505 20. https://www.upmet.com/products/titanium/cp-grade-2 (accessed on 25th June 2019).
506 21. Gouzman, I.; Dubey, M.; Carolus, M.D.; Schwartz, J.; Bernasek, S.I.; Monolayer vs. multilayer
507   self-assembled alkylphosphonate films: X-ray photoelectron spectroscopy studies. *Surf. Sci.* **2006**, *600*,
508   773-781., doi: 10.1016/j.susc.2005.11.030.
509 22. Petrović, Ž.; Katić, J.; Metikoš-Huković, M.; Dadafarin, H.; Omanovic, S. Modification of a Nitinol Surface
510   by Phosphonate Self-Assembled Monolayers. *J. Electrochem. Soc.* **2011**, *158*, F159-F165., doi:
511   10.1149/1.3617651.
512 23. Mellado-Valero, A.; Muñoz, A.I.; Pina, V.G.; Sola-Ruiz, M.F. Electrochemical Behaviour and Galvanic
513   Effects of Titanium Implants Coupled to Metallic Suprastructures in Artificial Saliva. *Materials* **2018**, *11*
514   171-190., doi: 10.3390/ma11010171.
515 24. Boukamp, A. A Nonlinear Least Squares Fit procedure for analysis of immittance data of electrochemical
516   systems. *Solid State Ionics* **1986**, *20*, 31-44., doi: 10.1016/0167-2738(86)90031-7.
517 25. Gaussian 09, Revision D.01, Frisch, M.J.; Trucks, G.W.; Schlegel, H.B.; Scuseria, G.E.; Robb, M.A.;
518   Cheeseman, J.R.; Scalmani, G.; Barone, V.; Mennucci, B.; Petersson, G.A.; Nakatsuji, H.; Caricato, M.; Li, X.;
519   Hratchian, H.P.; Izmaylov, A.F.; Bloino, J.; Zheng, G.; Sonnenberg, J.L.; Hada, M.; Ehara, M.; Toyota, K.;
520   Fukuda, R.; Hasegawa, J.; Ishida, M.; Nakajima, T.; Honda, Y.; Kitao, O.; Nakai, H.; Vreven, T.;
521   Montgomery, Jr., J.A.; Peralta, J. E.; Ogliaro, F.; Bearpark, M.; Heyd, J.J.; Brothers, E.;. Kudin, K.N.;
522   Staroverov, V.N.; Kobayashi, R.; Normand, J.; Raghavachari, K.; Rendell, A.; Burant, J.C.; Iyengar, S.S.;
523   Tomasi, J.; Cossi, M.; Rega, N.; Millam, J.M.; Klene, M.; Knox, J.E.; Cross, J.B.; Bakken, V.; Adamo, C.;

Jaramillo, J.; Gomperts, R.; Stratmann, R.E.; Yazyev, O.; Austin, A.J.; Cammi, R.; Pomelli, C.; Ochterski, J.W.; Martin, R.L.; Morokuma, K.; Zakrzewski, V.G.; Voth, G.A.; Salvador, P.; Dannenberg, J.J.; Dapprich, S.; Daniels, A.D.; Farkas, Ö.; Foresman, J.B.; Ortiz, J.V.; Cioslowski, J.; Fox, D.J. Gaussian, Inc., Wallingford CT, 2013.

26.   Allard, M.M.; Merlos, S.N.; Springer, B.N.; Cooper, J.; Zhang, G.; Boskovic, D.S.; Kwon, S.R.; Nick, K.E.; Perry, C.C. Role of TiO_2 Anatase Surface Morphology on Organophosphorus Interfacial Chemistry. *J. Phys. Chem. C* **2018**, *122*, 29237–29248., doi: 10.1021/acs.jpcc.8b08641.

27.   Qu, Z.; Kroes, G.-J. Theoretical Study of Stable, Defect-Free $(TiO_2)n$ Nanoparticles with n = 10–16. *J. Phys. Chem. C* **2007**, *111*, 16808–16817., doi: 10.1021/jp073988t.

28.   Zhao, Y.; Thrular, D.G. The M06 suite of density functionals for main group thermochemistry, thermochemical kinetics, noncovalent interactions, excited states, and transition elements: two new functionals and systematic testing of four M06-class functionals and 12 other functionals. *Theor. Chem. Acc.* **2008**, *120*, 215-241., doi: 10.1007/s00214-007-0310-x.

29.   Zhao, Y.; Truhlar, D.G. Density Functionals with Broad Applicability in Chemistry. *Acc. Chem. Res.* **2008**, *41*, 157–167., doi:10.1021/ar700111a.

30.   Zhao, Y.; Truhlar, D.G. Density Functional Theory for Reaction Energies: Test of Meta and Hybrid Meta Functionals, Range-Separated Functionals, and Other High-Performance Functionals. *J. Chem. Theory Comput.* **2011**, *7*, 669–676., doi:10.1021/ct1006604.

31.   Wadt, W.R.; Hay, P.J. Ab initio effective core potentials for molecular calculations. Potentials for main group elements Na to Bi. *J. Chem. Phys.* **1985**, *82*, 284–298., doi:10.1063/1.448800.

32.   Marenich, A.V.; Cramer, C.J.; Truhlar, D.G. Universal Solvation Model Based on Solute Electron Density and on a Continuum Model of the Solvent Defined by the Bulk Dielectric Constant and Atomic Surface Tensions. *J. Phys. Chem. B* **2009**, *113*, 6378–6396., doi.org/10.1021/jp810292n.

33.   Keith, T.A. *AIMAll (Version 17.01.25)*, TK Gristmill Software, Overland Park KS, USA, 2017 (aim.tkgristmill.com)

34.   Bader, R.F.W. *Atoms in Molecules: A Quantum Theory*, Oxford University Press, Oxford, New York, USA, 1994.

35.   Rupp, F.; Scheideler, L.; Rehbein, D.; Axmann, D.; Geis-Gerstorfer, J. Roughness induced dynamic changes of wettability of acid etched titanium implant modifications. *Biomaterials* **2004**, *25*, 1429-1438., doi: 10.1016/j.biomaterials.2003.08.015.

36.   Webster, T.J.; Ejiofor, J.U. Increased osteoblast adhesion on nanophase metals: Ti, Ti6Al4V, and CoCrMo. *Biomaterials* **2004**, *25*, 4731-4739., doi: 10.1016/j.biomaterials.2003.12.002.

37.   Ferreira, C.C.; Pereira Ricci, V.; de Sousa, L.L.; Marianoa, N.A.; Campos, M.G.N. Improvement of Titanium Corrosion Resistance by Coating with Poly-Caprolactone and Poly-Caprolactone/Titanium Dioxide: Potential Application in Heart Valves. *Mater. Res.* **2017**, *20*, 126-133., doi: 10.1590/1980-5373-MR-2017-0425.

38.   Ingole, P.G.; Baig, M.I.; Choi, W.K.; Lee, H.K. Synthesis and characterization of polyamide/polyester thin-film nanocomposite membranes achieved by functionalized TiO_2 nanoparticles for water vapor separation. *J. Mater. Chem. A* **2016**, *4*, 5592-5604., doi:10.1039/C6TA00100A.

39.   Othayoth, R.; Mathi, P.; Bheemanapally, K.; Kakarla, L.; Botlagunta, M. Characterization of vitamin–cisplatin-loaded chitosan nano-particles for chemoprevention and cancer fatigue. *J. Microencapsul.* **2015**, *32*, 1–11., doi: 10.3109/02652048.2015.1065921.

40.   Orazem, M.E.; Tribollet, B. *Electrochemical Impedance Spectroscopy*, John Wiley & Sons, New York, USA, 2008; pp. 233-265.

41.   Brug, G. J.; van den Eeden, A. L. G.; Sluyters-Rehbach, M.; Sluyters, J. H. The analysis of electrode impedances complicated by the presence of a constant phase element. *J. Electroanal. Chem. Interfacial Electrochem.* **1984**, *176*, 275–295., doi:10.1016/S0022-0728(84)80324-1.

42.   Jorcin, J.B.; Orazem, M.E.; Pébère, N.; Tribollet, B. CPE analysis by local electrochemical impedance spectroscopy. *Electrochim. Acta* **2006**, *51*, 1473–1479., doi:10.1016/j.electacta.2005.02.128.

43.   Pan, J.; Thierry, D.; Leygraf, C. Electrochemical impedance spectroscopy study of the passive oxide film on titanium for implant application. *Electrochim. Acta* **1996**, *41*, 1143-1153., doi: 10.1016/0013-4686(95)00465-3.

44.   Kosec, T.; Legat, A.; Kovač, J.; Klobčar, D., Influence of Laser Colour Marking on the Corrosion Properties of Low Alloyed Ti.*Coatings 2019, 9*, 375-389., doi:10.3390/coatings9060375

45. Aziz-Kerrzo, M.; Conroy, K.G.; Fenelon, A.M.; Farrell, S.T.; Bresllin, C.B. Electrochemical studies on the stability and corrosion resistance of titanium-based implant materials, *Biomaterials* **2001**, *22*, 1531-1539., doi: 10.1016/S0142-9612(00)00309-4.

46. de Assis, S.L.; Wolynec, S.; Costa, I. Corrosion characterization of titanium alloys by electrochemical techniques. *Electrochim. Acta* **2006**, *51*, 1815-1819., doi: 10.1016/j.electacta.2005.02.121.

47. Qu, Q.; Wang, L.; Chen, Y.; Li, L.; He,Y.; Ding, Z. Corrosion Behavior of Titanium in Artificial Saliva by Lactic Acid. *Materials* **2014**, *7*, 5528-5542., doi: 10.3390/ma7085528.

48. Guo, X.; Shi, H.; Xi, L. Corrosion and Electrochemical Impedance Properties of Ti Alloys as Orthopaedic Trauma Implant Materials. *Int. J. Electrochem. Sci.* **2017**, *12*, 9007-9016., doi: 10.20964/2017.10.05.

49. Mishnaevsky, L.; Levashov, E.; Valiev, R.Z., Segurado, J.; Sabirov, I.; Enikeev, N.; Prokoshkin, S.; Solov'yov, A.V.; Korotitskiy, A.; Gutmanas, E.; Gotman, I.; Rabkin, E.; Psakhe, S.; Dluhos, L.; Seefeldt, M.; Smolin, A. Nanostructured titanium-based materials for medical implants: Modeling and development. *Mater. Sci. Eng. R* **2014**, *81*, 1-19., doi:10.1016/j.mser.2014.04.002.

50. Scully, J. R. Polarization Resistance Method for Determination of Instantaneous Corrosion Rates. *CORROSION* **2000**, *56*, 199–218., doi:10.5006/1.3280536.

51. Tamilselvi, S.; Murugaraj, R.; Rajendran, N. Electrochemical impedance spectroscopic study of titanium and its alloys in saline medium. *Mater. Corros.* **2007**, *58*, 113-120., doi:10.1002/maco.200603979.

52. Evans, D.; Urankar, E.; Ulman, A.; Ferris, N. Self-assembled monolayers of alkanethiols containing a polar aromatic group: effects of the dipole position on molecular packing, orientation, and surface wetting properties. *J. Am. Chem. Soc.* **1991**, *113*, 4121-4131., doi:10.1021/ja00011a010.

53. Boubour, E.; Lennox, R.B. Insulating Properties of Self-Assembled Monolayers Monitored by Impedance Spectroscopy. *Langmuir* **2000**, *16*, 7464-7470., doi:10.1021/la991328c.